Journal of Zhejiang University SCIENCE A
ISSN 1673-565X (Print); ISSN 1862-1775 (Online)
www.zju.edu.cn/jzus; www.springerlink.com
E-mail: jzus@zju.edu.cn

Integrated phase unwrapping algorithm for the measurement of 3D shapes by Fourier transform profilometry*

Shuang-qing WU†, Yin ZHANG†‡, San-yuan ZHANG, Xiu-zi YE

(*School of Computer Science and Technology, Zhejiang University, Hangzhou 310027, China*)

†E-mail: wsqing1999@163.com; yinzh@cs.zju.edu.cn

Received Aug. 30, 2008; Revision accepted Dec. 9, 2008; Crosschecked Apr. 28, 2009

Abstract: An integrated and reliable phase unwrapping algorithm is proposed based on residues and blocking-lines detection, closed contour extraction and quality map ordering for the measurement of 3D shapes by Fourier-transform profilometry (FTP). The proposed algorithm first detects the residues on the wrapped phase image, applies wavelet analysis to generate the blocking-lines that can just connect the residues of opposite polarity, then carries out the morphology operation to extract the closed contour of the shape, and finally uses the modulation intensity information and the Laplacian of Gaussian operation of the wrapped phase image as the quality map. The unwrapping process is completed from a region of high reliability to that of low reliability and the blocking-lines can prevent the phase error propagation effectively. Furthermore, by using the extracted closed contour to exclude the invalid areas from the phase unwrapping process, the algorithm becomes more efficient. The experiment shows the effectiveness of the new algorithm.

Key words: Fourier-transform profilometry (FTP), Phase unwrapping, Residues, Blocking-lines, Laplacian of Gaussian, Modulation intensity

doi:10.1631/jzus.A0820630 **Document code:** A **CLC number:** TP391

INTRODUCTION

Optical 3D sensing techniques based on structured illumination have been widely studied in scientific fields and can be applied to surface topography, industrial inspection, quality control, biomedicine, machine vision, and so on (Huang *et al.*, 1999; 2002; Chen *et al.*, 2000; Dipanda and Woo, 2005; Zhang and Yau, 2006; Su *et al.*, 2008). Fourier-transform profilometry (FTP) is one of the most popular optical 3D sensing techniques. It has the advantages of full-field acquisition, fast processing, high resolution, non-contact operation, and only one fringe pattern is needed (Takeda and Mutoh, 1983; Su and Chen, 2001; Kemao, 2007; Iwata *et al.*, 2008).

The phase information modulated in the fringe pattern corresponds to the shape (height) of the object under measurement in FTP. However, the phase obtained is a wrapped phase whose principal value ranges from $-\pi$ to π, so phase unwrapping should be carried out to restore the unknown multiple of 2π to each pixel to retrieve the natural phase. The key to reliable phase unwrapping is the ability to detect the 2π jumps in the wrapped phase image accurately. The speckle-like noise, local shadow and the excessive density or sparsity of the fringe distribution are the major obstacles to correct phase unwrapping. Phase unwrapping remains a crucial and challenging problem in the accurate measurement of 3D shapes.

Goldstein *et al*.(1988)'s branch cut algorithm defined branch cuts between all detected residues to prevent any phase unwrapping path from crossing these cuts. Gutmann and Weber (2000), Lu *et al*.(2005), and Karout *et al*.(2007) also applied the detected branch cuts to set barriers for the phase unwrapping process. These path-following algorithms

‡ Corresponding author

* Project (Nos. 2007AA04Z1A5 and 2007AA01Z311) supported by the Hi-Tech Research and Development Program (863) of China

lack the weighting factors that could be used for guiding the placement of branch cuts and would result in a poor performance in areas of low coherence and in areas with densely placed branch cuts.

The quality guide algorithms do not identify residues at all; they rely completely on a quality map to determine the order in which the phase data are unwrapped. The quality map can be defined as the phase derivative variances (Herráez *et al.*, 2002; Zhang *et al.*, 2007), modulation intensity (Su and Xue, 2001; Quan *et al.*, 2003; Su and Chen, 2004), and the amplitude of wavelet transform coefficients at the wavelet-ridge position (Li *et al.*, 2008).

Ghiglia and Pritt (1998) provided a review of phase unwrapping algorithms. In (Zappa and Busca, 2008) the performances of eight different phase unwrapping algorithms (representative of the two main unwrapping methodologies) in the specific application of FTP are compared according to the phase unwrapping errors, execution time, and the accuracy of the reconstructed shape in comparison with the real objects.

The integrated and reliable phase unwrapping algorithm proposed in this paper can be regarded as a cross between the path-following algorithm and the quality guide algorithm. The characteristics and contributions of this method are summarized as follows.

(1) The application of the correlation between the local modulus maxima of wavelet coefficients and the local singularity to trace the blocking-lines in the wrapped phase image, which can effectively balance the detected residues of opposite polarity and prevent the phase error propagation.

(2) The application of the wavelet analysis and morphology operation to extract the closed contour of the shape so as to exclude invalid areas from the phase unwrapping process to make the algorithm more efficient.

(3) Using the modulation intensity information and the Laplacian of Gaussian operation of the wrapped phase image to guide phase unwrapping, the phase unwrapping process is completed from a region of high reliability to a region of low reliability.

The remainder of the paper is organized as follows. Section 2 introduces the basic principle of FTP. The detailed description of the proposed integrated and reliable phase unwrapping algorithm for the measurement of 3D shapes by FTP is introduced in Section 3. Section 4 gives the experiment result of the proposed algorithm applied to the measurement of 3D shapes by FTP. We summarize the conclusions in Section 5.

PRINCIPLE OF FTP

Here we briefly review the fundamental principle of the FTP, which was first introduced by Takeda and Mutoh (1983). In the FTP, a grating image is projected to a reference plane, and the image on the reference plane obtained by the CCD camera can be written as

$$g_0(x,\ y)=\sum_{n=-\infty}^{\infty}A_n\exp\left\{\mathrm{j}\left[2\pi nf_0x+n\varphi_0(x,y)\right]\right\},\quad(1)$$

where A_n is the frequency intensity, the x axis is perpendicular to the direction of the grating fringes, the y axis is parallel to that direction, f_0 is the fundamental frequency of the grating image, $f_0=1/p_0=\cos\theta/p$, and $\varphi_0(x, y)$ is the initial phase modulation. Then the same grating image is projected to the 3D shape which is placed on the reference plane, and the deformed grating image obtained by the CCD camera can be written as

$$g(x,\ y)=r(x,y)\sum_{n=-\infty}^{\infty}A_n\exp\left\{\mathrm{j}\left[2\pi nf_0x+n\varphi(x,y)\right]\right\},\quad(2)$$

where $r(x, y)$ represents the reflecting property of the surface of the object under measurement.

Applying the Fourier transformation to $g(x, y)$ to compute its frequency spectrum, of which the zero frequency represents the background illumination and the fundamental frequency contains the shape (height) information of the object under measurement. By using a proper digital filter, the fundamental frequency can be retrieved. Then compute its inverse Fourier transform to obtain the following signal that contains the fundamental frequency:

$$g'(x,y)=A_1r(x,y)\exp\left\{\mathrm{j}[2\pi f_0x+\varphi(x,y)]\right\}.\quad(3)$$

The same operation is applied to $g_0(x, y)$ and we obtain

$$g_0'(x,y)=A_1\exp\{\mathrm{j}[2\pi f_0 x+\varphi_0(x,y)]\}. \quad (4)$$

The phase difference is $\Delta\varphi(x, y)=\varphi(x, y)-\varphi_0(x, y)$. Through system calibration we can finally establish the mapping relation between the phase and height (Legarda-Sáenz *et al*., 2004; Zhang and Huang, 2006).

However, the phase difference calculated above is a wrapped phase, whose principal value ranges from $-\pi$ to π. Before system calibration, phase unwrapping should be carried out to restore the unknown multiple of 2π to each pixel to retrieve the natural phase.

INTEGRATED PHASE UNWRAPPING ALGORITHM

The phase unwrapping algorithm proposed in this research consists of three main parts: residues and blocking-lines detection to prevent the phase error propagation, closed contour extraction to exclude the invalid areas from the phase unwrapping, and the modulation intensity information and the Laplacian of Gaussian operation of the wrapped phase image ordering to guide the direction of the phase unwrapping.

Residues and blocking-lines detection

1. Residues detection

The residue concept forms the basis for virtually all path-following phase unwrapping methods. From Green's function in calculus theory and 2D phase unwrapping theory, phase unwrapping aims at calculating the line integral formula:

$$\varphi(r)=\oint_C \Delta\varphi \mathrm{d}r+\varphi(r_0), \quad (5)$$

where C is a random path in the domain D that connects the point r and the point r_0, and $\Delta\varphi$ is the gradient of the phase value φ.

According to the residue theorem of 2D phase unwrapping, we can judge whether a point is a residue or not by selecting a path C that contains its 3×3 neighbor as shown in Fig.1.

Calculate the gradient of the wrapped phase image along the path C, which is expressed as

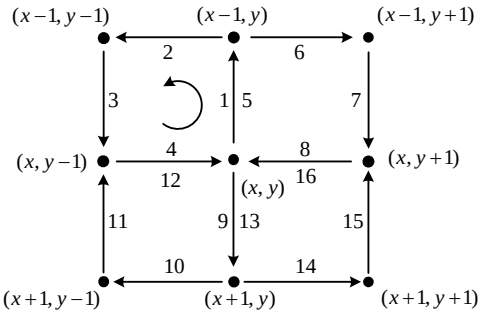

Fig.1 Path for residues detection

$$\begin{aligned}
&\Delta_1=R((\varphi(x,y)-\varphi(x-1,y))/(2\pi)),\\
&\Delta_2=R((\varphi(x-1,y)-\varphi(x-1,y-1))/(2\pi)),\\
&\Delta_3=R((\varphi(x-1,y-1)-\varphi(x,y-1))/(2\pi)), \quad (6)\\
&\ldots\\
&\Delta_{16}=R((\varphi(x,y+1)-\varphi(x,y))/(2\pi)),
\end{aligned}$$

where $R(x)$ means the nearest integer of x. Finally, calculate the integral value S, which is expressed as

$$S=\sum_{i=1}^{16}\Delta_i. \quad (7)$$

The pixel on the wrapped phase image is a residue if S is not equal to 0. If $S>0$, then the pixel is a positive residue; if $S<0$, it is a negative residue.

Fig.2a is a simulated peak mesh with shadow, distortion and noise, and Figs.2b and 2c show its deformed grating image and the detected residues distribution on the wrapped phase image, respectively.

In the path-following phase unwrapping algorithms, if the residues can be balanced by connecting the residue of opposite polarity, phase unwrapping can be carried out along any path that does not cross these connecting lines. However, it is still a very difficult task to connect the residues of opposite polarity either by the cut-lines or by the curve-lines.

2. Blocking-lines detection

The blocking-lines correspond to the unreliable regions of the wrapped phase image due to the speckle-like noise, local shadow or abrupt changes in the height, and so on. So there is a strong correlation between the local spatial frequency of the wrapped phase image and the position of the blocking-lines.

In our method, the correlation between the local modulus maxima of wavelet coefficients and the local

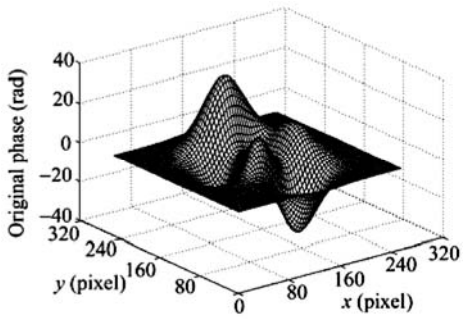

(a)

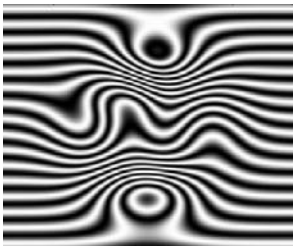

(b)

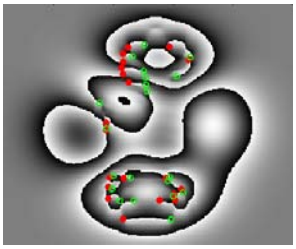

(c)

Fig.2 Residues detection

(a) A simulated peak mesh with shadow, distortion and noise; (b) The deformed grating image; (c) The detected residues distribution on the wrapped phase image, of which the points indicate the positive residues and the circles indicate the negative residues

singularity is applied to trace the blocking-lines that can effectively balance the residues with opposite polarity. The Morlet wavelet consisting of a sine wave and cosine wave modulated by a Gaussian function can provide better localization in both spatial and frequency domains (Gdeisat *et al.*, 2006). The 1D complex Morlet wavelet could be expressed as

$$\varphi(x)=\frac{1}{\sqrt[4]{\pi}}\sqrt{\frac{2\pi}{\sigma}}\exp\left[-\frac{(2\pi/\sigma)^2x^2}{2}+\mathrm{j}2\pi x\right], \quad (8)$$

where $\sigma=(2/\ln 2)^{1/2}\pi$, and the daughter wavelets $\varphi_{a,b}(x)$ are built by translation on the x axis by b and dilation by a of the mother wavelet, which is given by

$$\varphi_{a,b}(x)=\frac{1}{\sqrt{a}}\varphi\left(\frac{x-b}{a}\right)=\frac{1}{\sqrt[4]{\pi}}\sqrt{\frac{2\pi}{a\sigma}}\exp\left[\mathrm{j}2\pi\left(\frac{x-b}{a}\right)\right]\exp\left[-\frac{2\pi^2}{\sigma^2}\left(\frac{x-b}{a}\right)^2\right]. \quad (9)$$

The continuous wavelet transform for the signal $f(x)$ can be expressed as

$$W(a,b)=\frac{1}{\sqrt{a}}\int_{-\infty}^{+\infty}\varphi_{a,b}^{*}\left(\frac{x-b}{a}\right)f(x)\mathrm{d}x, \quad (10)$$

where $\varphi_{a,b}^{*}(x)$ denotes the complex conjugate of the mother wavelet.

Apply the 2D wavelet transform to the wrapped phase image. The threshold of the wavelet coefficients is determined by residues distribution, to make the blocking-lines balance the detected residues of opposite polarity, that is to locate the detected residues just on the two side ends of the blocking-lines. Figs.3a and 3b show the detected blocking-lines and the residues distribution corresponding to the simulated peak mesh, respectively.

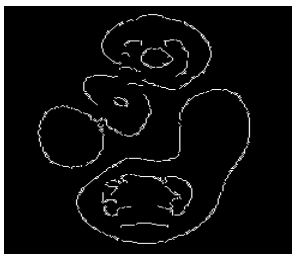

(a)

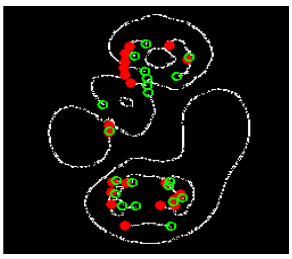

(b)

Fig.3 (a) Detected blocking-lines of the wrapped phase image; (b) Residues distribution

The points indicate the positive residues and the circles indicate the negative residues

In order to prevent the phase error propagating through the unwrapping path, we set a binary mask $m_1(x, y)$ defined in Eq.(11) that has the same size as the wrapped phase image to separate the regions corresponding to the blocking-lines, of which the phase cannot be properly unwrapped. The points whose mask value equals one indicate the blocking-line regions.

$$m_1(x,y)=\begin{cases}1, & \text{blocking-line region,}\\ 0, & \text{other region.}\end{cases} \quad (11)$$

Closed contour extraction

In the optical 3D sensing techniques based on structured illumination including the FTP method, the deformed grating image captured by the CCD camera usually contains some invalid background areas. Before phase unwrapping we should exclude these areas by extracting the closed contour of the shape under measurement. Zhang *et al.*(2007) extracted the background mask by setting the threshold value for

the histogram of the modulation intensity. The closed contour extraction is also a necessary and critical procedure in the multi-view 3D registration of range images.

The contour of the shape usually corresponds to the abrupt change in the height and can cause an abrupt change of the phase in the wrapped phase image. The Morlet wavelet introduced above is applied to extract the contour of the shape. The threshold of the wavelet coefficients is decreased gradually, until the contour of the shape has already been apparently detected.

The contour detected by the wavelet usually contains many isolated short sections. The image processing method of the morphological operation that handles the interior geometrical structure of the image is applied to form a closed contour (Baek *et al.*, 2003). The closing operation composed of dilation and erosion is carried out several times to close the contour, and the skeleton of the closed contour can be finally obtained through skeleton operation of morphological analysis.

The binary image f dilation with the structure element B is represented as

$$g_{\mathrm{d}}(x,y)=(f\oplus B)(x,y)=\bigcup_{(m,n)\in B} f(x-m,y-n), \quad (12)$$

and erosion operation is represented as

$$g_{\mathrm{e}}(x,y)=(f\Theta B)(x,y)=\bigcap_{(m,n)\in B} f(x+m,y+n). \quad (13)$$

The closing operation is to apply the dilation operation followed by the erosion operation:

$$(f\circ b)(x,y)=[(f\oplus B)\Theta B](x,y). \quad (14)$$

The skeleton of the contour edge in an image f is extracted by

$$S(A)=\bigcup_{k=0}^{K} S_k(f), \quad (15)$$

where

$$S_k(f)=(f\Theta kB)-[(f\Theta kB)\circ B],$$

$$K=\max\{k\mid (f\Theta kB)\neq\varnothing\},$$

and $(f\Theta kB)$ means to erosion image f with the structure element B by k times.

To improve the efficiency of the phase unwrapping, a new binary mask $m_2(x, y)$ defined in Eq.(16) is generated according to the extracted contour. The pixel whose mask value equals zero indicates the region outside the contour that contains the invalid areas, and the pixel whose mask value equals 1 indicates the region inside the contour that contains the valid fringe-pattern information.

$$m_2(x,y)=\begin{cases}0, & \text{outside the contour,}\\ 1, & \text{inside the contour.}\end{cases} \quad (16)$$

A final binary mask $m(x, y)$ is generated from $m_1(x, y)$ and $m_2(x, y)$ to control the phase unwrapping process. The mathematical representation of this mask is expressed as

$$m(x,y)=m_1(x,y)\cup\overline{m_2(x,y)}. \quad (17)$$

Reliability ordering

The quality guided path unwrapping algorithms use different criteria to determine the reliability of the pixels on the wrapped phase image. The success or failure of a phase unwrapping relies on the availability of a good quality map. In our algorithm, two different quality maps, the modulation intensity and the Laplacian of Gaussian of the wrapped phase image ordering, are used.

1. The first quality map

The modulation intensity of the deformed grating image can be expressed as follows:

$$M(x,y)=\left|g'(x,y)\right|=A_1 r(x,y). \quad (18)$$

The modulation intensity is proportional to the surface brightness and fringe contrast, and reflects the accuracy and reliability of the measured phase. The value of the modulation function in the areas of local shadow and abrupt discontinuities is lower than that in other areas. So the modulation could be a useful quality map to determine an optimized phase unwrapping path.

$$Q_1(x,y)=M(x,y). \quad (19)$$

However, a modulation function cannot be responsible for the doubtful areas that have been corrupted by under-sampling when these pixels may

have good image quality and therefore higher modulation values (Su and Xue, 2001). To solve this problem, we use a second quality map as well to enhance the ordering of the reliability of the pixels on the wrapped phase image.

2. The second quality map

The gradient or difference between a pixel and its neighbors on the wrapped phase image is commonly employed as the quality map. Those points with the lowest module 2π gradients with respect to their neighbors are determined to be the most reliable points and, therefore, are processed first. And the use of the Laplacian of Gaussian can provide better location of the possible inconsistencies and abrupt changes in the wrapped phase image because of its attractive scaling properties (Gunn, 1999).

The 2D Gaussian of standard deviation σ is given by

$$G(x,y)=\frac{1}{2\pi\sigma^2}\exp\left(-\frac{x^2+y^2}{2\sigma^2}\right). \quad (20)$$

The Laplacian of Gaussian is given by

$$\nabla^2 G(x,y)=\frac{\partial^2 G}{\partial x^2}+\frac{\partial^2 G}{\partial y^2}=\frac{1}{2\pi\delta^4}\left(\frac{x^2+y^2}{\delta^2}-2\right)\exp\left(-\frac{x^2+y^2}{2\delta^2}\right). \quad (21)$$

The quality map $Q_2(x, y)$ is obtained by convolving the wrapped phase image $f(x, y)$ with the Laplacian of Gaussian

$$Q_2(x,y)=f(x,y)\otimes\nabla^2 G(x,y). \quad (22)$$

The final reliability of the point on the wrapped phase image is determined by

$$R(x,y)=\alpha Q_1(x,y)+\beta/Q_2(x,y), \quad (23)$$

where the weight factors α and β depend on the quality of the modulation intensity map and the quality of the Laplacian of Gaussian quality map, respectively.

In the proposed phase unwrapping algorithm, an ordering queue and two binary masks are employed. The pixels to be unwrapped are placed in order in the ordering queue according to their quality values. The binary mask $M_1(x, y)$ is set to be equal to the mask $m(x, y)$ that is generated in Eq.(17), and all the initial values in the binary mask $M_2(x, y)$ are set to be zero, showing that its phase has not been unwrapped. The algorithm operates as follows:

Step 1: Select a point with the highest quality value as the starting point, and set the corresponding point on the binary masks $M_1(x, y)$ and $M_2(x, y)$ as 1. Its four neighbors are examined. The neighboring points whose values on the binary mask $M_1(x, y)$ are 0 will be sent to the ordering list.

Step 2: Select the maximum point from the ordering queue, unwrap this point by comparing the phase with one of its neighboring pixels whose values on the mask $M_2(x, y)$ are 1, then set the newly wrapped point on the binary masks $M_1(x, y)$ and $M_2(x, y)$ as 1, remove the newly wrapped point from the ordering queue and examine its four neighbors, and send its neighboring points whose values on the binary mask $M_1(x, y)$ are 0 to the ordering list.

Step 3: Repeat Step 2, until the ordering queue is empty, and it means all the reliable points have been unwrapped.

Step 4: The phase value on the blocking-lines can be obtained by interpolating its neighboring pixels, while the phase value of the region outside the contour that corresponds to the invalid background can be discarded.

EXPERIMENT AND RESULT

Computer simulations and experiments are adopted to verify the reliability of the proposed phase unwrapping algorithm. The simulated object (the 3D mesh is shown in Fig.2a) is represented by the peak function, which is useful for demonstrating a complex object with abrupt discontinuities at the surface. Its mathematical expression (the parameters a_1, a_2 and a_3 can be adjusted to form the different complex shapes) is as follows:

$$\begin{aligned}peaks(x,y)=&\,a_1(1-x)^2\exp(-x^2-(y+1)^2)\\&-a_2(x/5-x^3-y^5)\exp(-x^2-y^2)\\&-a_3\exp(-(x-1)^2-y^2).\end{aligned} \quad (24)$$

Fig.4a shows the reconstructed peak and the error distribution by the conventional 2D phase

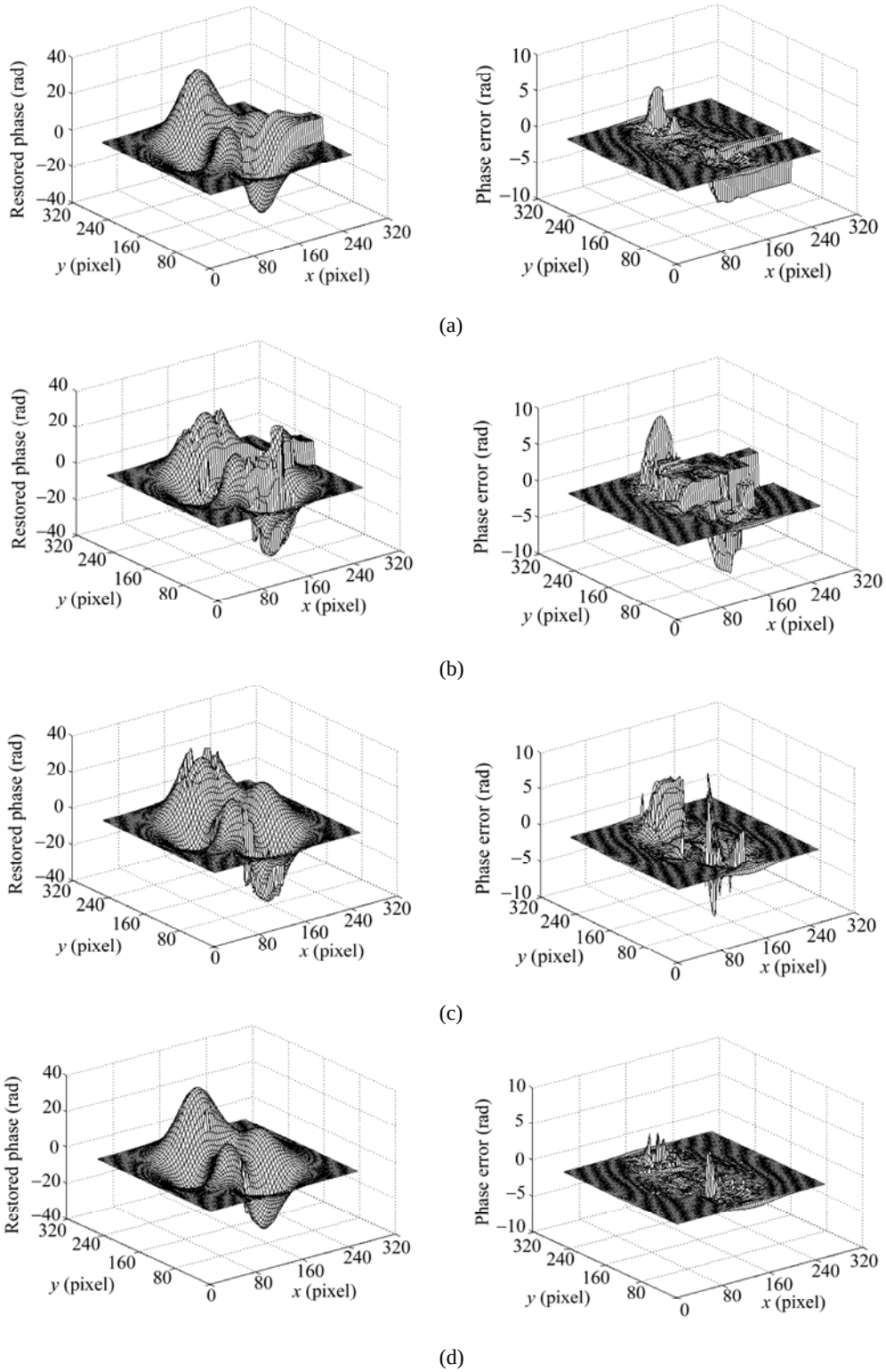

Fig.4 Restored peak and the error distribution

(a) By the conventional 2D phase unwrapping algorithm; (b) By the branch-cut phase unwrapping algorithm; (c) By the digital weighted filtering based modulation intensity ordering phase unwrapping algorithm; (d) By the proposed integrated phase unwrapping algorithm

unwrapping algorithm (neither the binary mask nor the quality is used), its mean absolute error is about 1.8494 rad. Fig.4b shows the reconstructed peak and the error distribution by the branch-cut phase unwrapping algorithm (without the quality map), its mean absolute error is about 1.6901 rad. Fig.4c shows the reconstructed peak and the error distribution by digital weighted filtering based modulation intensity ordering phase unwrapping algorithm (without the binary mask) (Su and Xue, 2001), its mean absolute error is about 0.3489 rad. Fig.4d shows the reconstructed peak and the error distribution by the proposed integrated phase unwrapping algorithm, its mean absolute error is about 0.1153 rad. Although the wrapped phase image contains shadow, distortion and noise, the whole shape of the simulated peak is properly reconstructed by our algorithm, and the mean absolute error is much smaller than the results restored by other algorithms.

In our experiment, a complex 3D shape is measured. The measurement system consists of a digital projector (Epson EMP730), a CCD camera (MINTRON-1881EX), an image grabber card (DH-CG410) and a processor, and it conforms to the conventional crossed-optical-axes geometry system as shown in Fig.5. The optical axes of the projector lens $E_p'E_p$ crosses with the optical axis of the camera E_cE_c', at point O on a reference plane R; d is the distance between the exit pupil of projector and the entrance pupil of the camera; l is the distance between the entrance pupil of the camera and the reference plane; p is the grating period. The deformed grating image captured by the CCD camera and the wrapped phase image are shown in Fig.6a and Fig.6b, respectively. The image size is 512×512 pixels, and the value is normalized from 0 to 255 as the gray scale images.

The detected blocking-lines and residues distribution in the wrapped phase image are shown in Fig.7a and Fig.7b, respectively. We can see that the blocking-lines detected by the method of local modulus maxima of wavelet coefficients can balance the residues of opposite polarity effectively. And the skeleton of the closed contour detected by wavelet analysis and morphological operation is shown in Fig.7c. Fig.7d shows the extracted close contour, as the face of the shape under measurement is selected for 3D reconstruction; the hat area located on the right side of the wrapped phase image is discarded just by putting a cutting line to the detected contour.

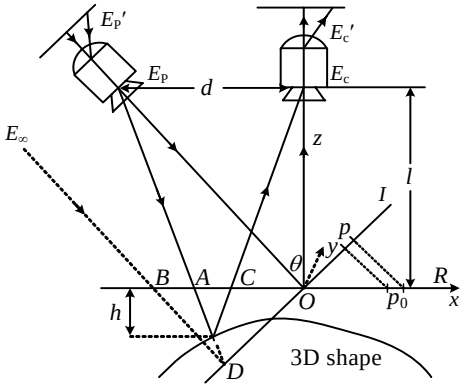

Fig.5 3D measurement system in FTP

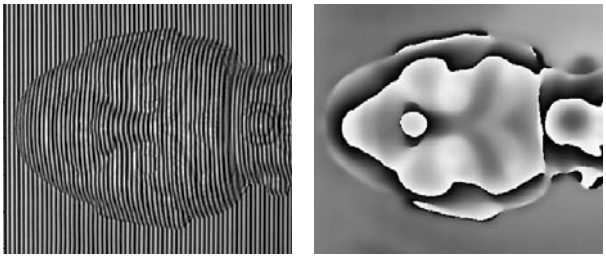

(a) (b)

Fig.6 Example for testing the proposed phase unwrapping algorithm. (a) Deformed grating image; (b) Wrapped phase image

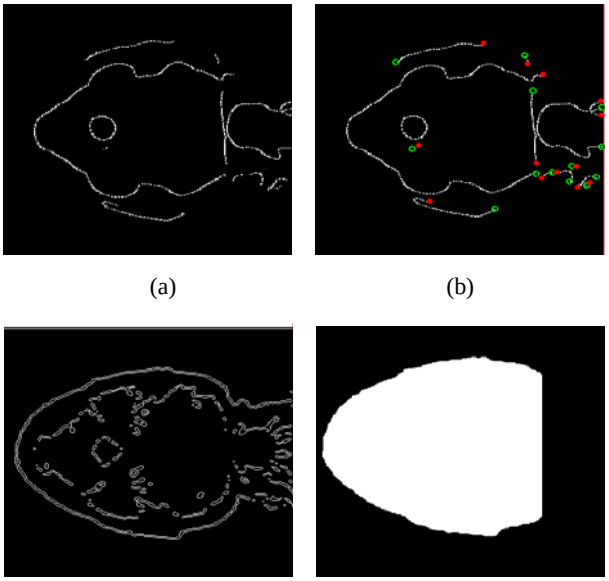

(a) (b)

(c) (d)

Fig.7 Blocking-lines detection and closed contour extraction. (a) Detected blocking-lines; (b) Residues distribution; (c) Skeleton of the contour; (d) Extracted closed contour

The binary mask $m(x, y)$ obtained by combining the detected blocking-lines and the extracted contour is shown in Fig.8. The pixels whose values on the binary mask equal 0 signify that the points could be wrapped, while the pixels whose values on the binary mask equal 1 signify that the points correspond to the blocking-lines or the invalid outside regions, and should be worked around during phase unwrapping.

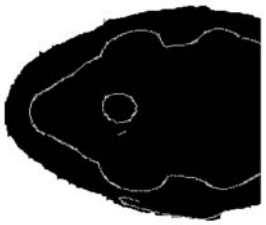

Fig.8 Binary mask obtained by combining the detected blocking-lines and the extracted closed contour

The quality map of modulation intensity information and the quality map of the Laplacian of Gaussian for the wrapped phase image are shown in Fig.9a and Fig.9b, respectively. The black value on the modulation intensity means low reliability, while the white value on the Laplacian of Gaussian for the wrapped phase image means low reliability.

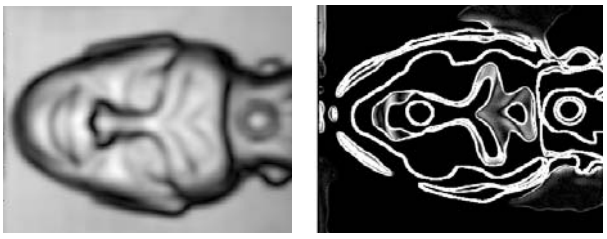

(a) (b)

Fig.9 Quality maps

(a) Modulation intensity; (b) Laplacian of Gaussian for the wrapped phase image

Two intermediate phase unwrapping steps by the proposed phase unwrapping algorithm are shown in Fig.10. The pixel whose phase has been unwrapped, the corresponding pixel on the binary mask changed from black to white. The phase unwrapping is completed from a region of high reliability to a region of low reliability, the pixels on the blocking-lines are walked around, and the regions outside the contour is not carried out during the phase unwrapping process.

Fig.11 shows the comparison between the phase unwrapping results using four different algorithms. The height value is demonstrated by the different gray values. It clearly shows that the conventional 2D phase unwrapping algorithm and the branch-cut phase unwrapping algorithm cannot unwrap the phase correctly. And our algorithm can obtain similar geometry to the digital weighted filtering based modulation intensity ordering phase unwrapping algorithm. However, as shown in Fig.11d, our algorithm can obtain a more accurate phase result in the detailed regions such as the two eyebrow areas.

(a) (b)

Fig.10 Two phase-unwrapping steps by the proposed unwrapping algorithm. (a) The first step; (b) The second step

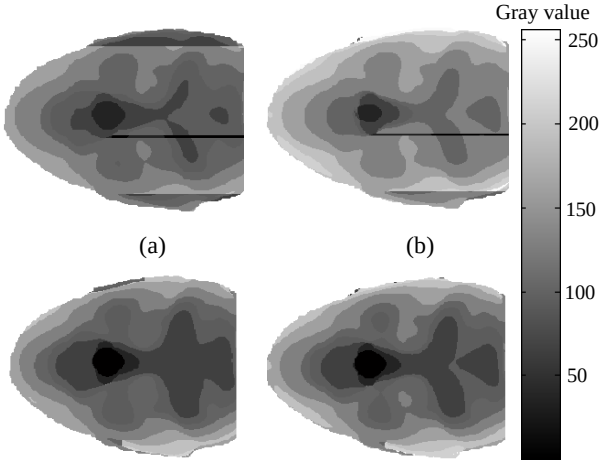

(a) (b)

(c) (d)

Fig.11 Results of the phase unwrapped by four different phase unwrapping algorithms

(a) Result by the conventional 2D phase unwrapping algorithm; (b) Result by the branch-cut phase unwrapping algorithm; (c) Result by the digital weighted filtering based modulation intensity ordering phase unwrapping algorithm; (d) Result by the proposed integrated phase unwrapping algorithm

Fig.12 shows the final reconstructed 3D shape from two different perspectives. The reconstructed shape is rendered by the OpenGL, and the holes under the nose are filled by the hole-filling algorithm (Jun, 2005). We can see that the whole face of the shape is properly obtained.

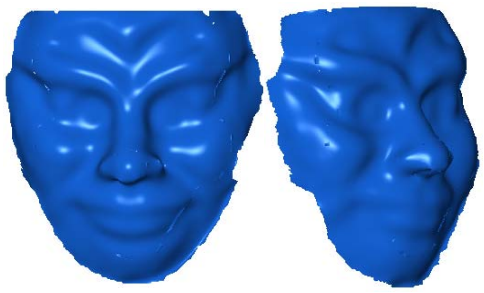

Fig.12 Reconstructed 3D shape viewed from two different perspectives

CONCLUSION

We presented an integrated and reliable phase unwrapping algorithm for the measurement of 3D shapes by FTP. The algorithm applies the blocking-lines in the wrapped phase image that can effectively balance the detected residues of opposite polarity to prevent phase error propagation, and then the closed contour is extracted to exclude the invalid areas from phase unwrapping. The quality map is generated from the modulation intensity information and the Laplacian of Gaussian operation of the wrapped phase image. The unwrapping process is completed from a region of high reliability to that of low reliability. The experiment shows the effectiveness and convenience of the new algorithm. More efficient interpolation algorithms to improve the accuracy of the data corresponding to the blocking-lines will be our future work.

References

Baek, Y.H., Byun, O.S., Moon, S.R., 2003. Image Edge Detection Using Adaptive Morphology Meyer Wavelet-CNN. Proc. Int. Joint Conf. on Neural Networks, **2**:1219-1222. [doi:10.1109/IJCNN.2003.1223866]

Chen, F., Brown, G.M., Song, M., 2000. Overview of three-dimensional shape measurement using optical methods. *Opt. Eng.*, **39**(1):10-22. [doi:10.1117/1.602438]

Dipanda, A., Woo, S., 2005. Towards a real-time 3D shape reconstruction using a structured light system. *Pattern Recogn.*, **38**(10):1632-1650. [doi:10.1016/j.patcog.2005.01.006]

Gdeisat, M.A., Burton, D.R., Lalor, M.J., 2006. Spatial carrier fringe pattern demodulation by use of a two-dimensional continuous wavelet transform. *Appl. Opt.*, **45**(34):8722-8732. [doi:10.1364/AO.45.008722]

Ghiglia, D.C., Pritt, M.D., 1998. Two-dimensional Phase Unwrapping: Theory, Algorithms, and Software. Wiley, New York.

Goldstein, R.M., Zebker, H.A., Werner, C.L., 1988. Satellite radar interferometry—two-dimensional phase unwrapping. *Radio Sci.*, **23**(4):713-720. [doi:10.1029/RS023i004p00713]

Gunn, S.R., 1999. On the discrete representation of the Laplacian of Gaussian. *Pattern Recogn.*, **32**(8):1463-1472. [doi:10.1016/S0031-3203(98)00163-0]

Gutmann, B., Weber, H., 2000. Phase unwrapping with the branch-cut method: role of phase-field direction. *Appl. Opt.*, **39**(26):4802-4816. [doi:10.1364/AO.39.004802]

Herráez, M.A., Burton, D.R., Lalor, M.J., Gdeisat, M.A., 2002. Fast two-dimensional phase-unwrapping algorithm based on sorting by reliability following a noncontinuous path. *Appl. Opt.*, **41**(35):7437-7444. [doi:10.1364/AO.41.007437]

Huang, P.S., Hu, Q., Jin, F., Chiang, F.P., 1999. Color-encoded digital fringe projection technique for high-speed three-dimensional surface contouring. *Opt. Eng.*, **38**(6):1065-1071. [doi:10.1117/1.602151]

Huang, P.S., Zhang, C., Chiang, F.P., 2002. High-speed 3-D shape measurement based on digital fringe projection. *Opt. Eng.*, **42**(1):163-168. [doi:10.1117/1.1525272]

Iwata, K., Kusunoki, F., Moriwaki, K., Fukuda, H., Tomii, T., 2008. Three-dimensional profiling using the Fourier transform method with a hexagonal grating projection. *Appl. Opt.*, **47**(12):2103-2108. [doi:10.1364/AO.47.002103]

Jun, Y., 2005. A piecewise hole filling algorithm in reverse engineering. *Computer-Aided Des.*, **37**(2):263-270. [doi:10.1016/j.cad.2004.06.012]

Karout, S.A., Gdeisat, M.A., Burton, D.R., Lalor, M.J., 2007. Residue vector, an approach to branch-cut placement in phase unwrapping: theoretical study. *Appl. Opt.*, **46**(21):4712-4727. [doi:10.1364/AO.46.004712]

Kemao, Q., 2007. Two-dimensional windowed Fourier transform for fringe pattern analysis: principles, applications and implementations. *Opt. Lasers Eng.*, **45**(2):304-317. [doi:10.1016/j.optlaseng.2005.10.012]

Legarda-Sáenz, R., Bothe, T., Jüptner, W.P., 2004. Accurate procedure for the calibration of a structured light system. *Opt. Eng.*, **43**(2):464-471. [doi:10.1117/1.1635373]

Li, S., Chen, W., Su, X., 2008. Reliability-guided phase unwrapping in wavelet-transform profilometry. *Appl. Opt.*, **47**(18):3369-3377. [doi:10.1364/AO.47.003369]

Lu, Y., Wang, X., He, G., 2005. Phase unwrapping based on branch cut placing and reliability ordering. *Opt. Eng.*, **44**(5):055601. [doi:10.1117/1.1911683]

Quan, C., Tay, C.J., Chen, L., Fu, Y., 2003. Spatial-fringe-modulation-based quality map for phase unwrapping. *Appl. Opt.*, **42**(35):7060-7065. [doi:10.1364/AO.42.007060]

Su, W.H., Kuo, C.Y., Wang, C.C., Tu, C.F., 2008. Projected fringe profilometry with multiple measurements to form an entire shape. *Opt. Expr.*, **16**(6):4069-4077. [doi:10.1364/OE.16.004069]

Su, X., Chen, W., 2001. Fourier transform profilometry: a

review. *Opt. Lasers Eng.*, **35**(5):263-284. [doi:10.1016/S0143-8166(01)00023-9]

Su, X., Xue, L., 2001. Phase unwrapping algorithm based on fringe frequency analysis in Fourier-transform profilometry. *Opt. Eng.*, **40**(4):637-643. [doi:10.1117/1.1355253]

Su, X., Chen, W., 2004. Reliability-guided phase unwrapping algorithm: a review. *Opt. Lasers Eng.*, **42**(3):245-261. [doi:10.1016/j.optlaseng.2003.11.002]

Takeda, M., Mutoh, K., 1983. Fourier transform profilometry for the automatic measurement of 3-D object shape. *Appl. Opt.*, **22**(24):3977-3982. [doi:10.1364/AO.22.003977]

Zappa, E., Busca, G., 2008. Comparison of eight unwrapping algorithms applied to Fourier-transform profilometry. *Opt. Lasers Eng.*, **46**(2):106-116. [doi:10.1016/j.oplaseng.2007.09.002]

Zhang, S., Huang, P.S., 2006. Novel method for structured light system calibration. *Opt. Eng.*, **45**(8):083601. [doi:10.1117/1.2336196]

Zhang, S., Yau, S.T., 2006. High-resolution, real-time 3D absolute coordinate measurement based on a phase-shifting method. *Opt. Expr.*, **14**(7):2644-2649. [doi:10.1364/OE.14.002644]

Zhang, S., Li, X., Yau, S.T., 2007. Multilevel quality-guided phase unwrapping algorithm for real-time three-dimensional shape reconstruction. *Appl. Opt.*, **46**(1):50-57. [doi:10.1364/AO.46.000050]